Electronic Supplementary Information

Microsteganography on All Inorganic Perovskite Micro-Platelets by Direct Laser Writing

Yuhang Sheng,[a] Cihui Liu,[a] Liyan Yu,[b] Yunyi Yang,[c] Fengrui Hu,[d] Chong Sheng,[d] Yunsong Di,[a] Lifeng Dong,[b] and Zhixing Gan*[a,b]

a. Center for Future Optoelectronic Functional Materials, School of Computer and Electronic Information/School of Artificial Intelligence, Nanjing Normal University, Nanjing 210023, China Email: zxgan@njnu.edu.cn
b. College of Materials Science and Engineering, Qingdao University of Science and Technology, Qingdao 266042, P. R. China
c. Faculty of Science, Engineering and Technology, Swinburne University of Technology, Hawthorn, VIC, 3122 Australia
d. National Laboratory of Solid State Microstructures, Nanjing University, Nanjing 210093, China

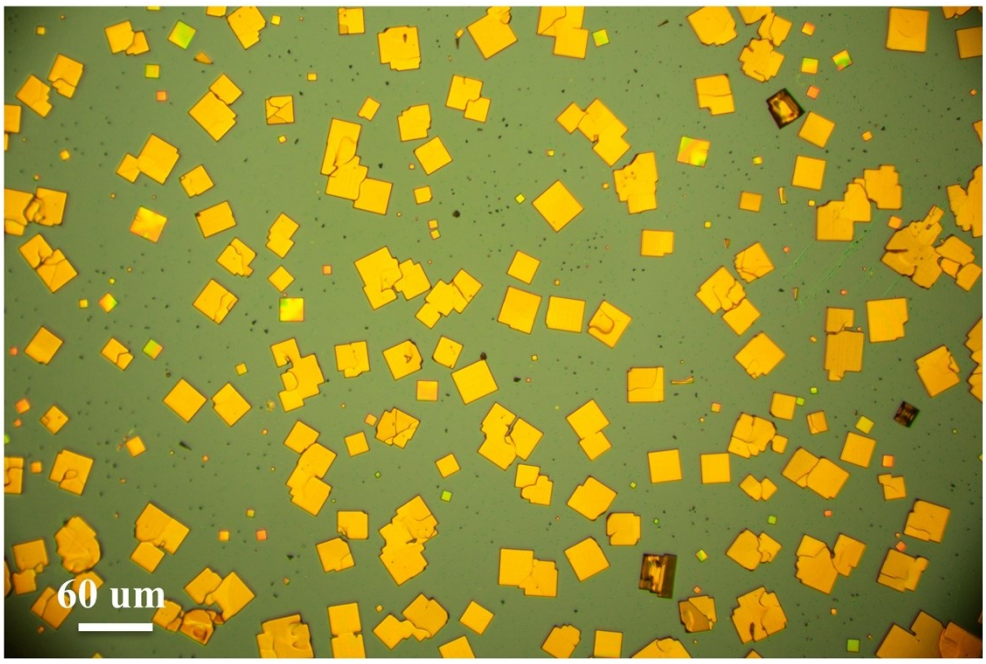

Figure S1. Low magnification OM image of the CVD-grown $CsPbBr_3$ MPs.

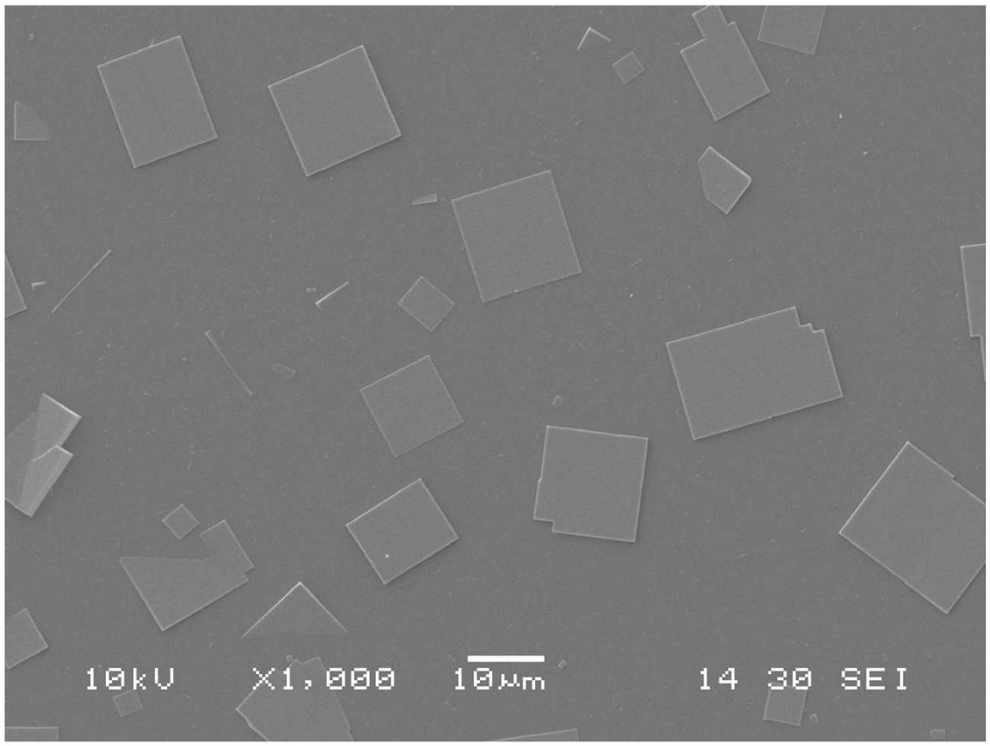

Figure S2. SEM image of the CVD-grown $CsPbBr_3$ MPs.

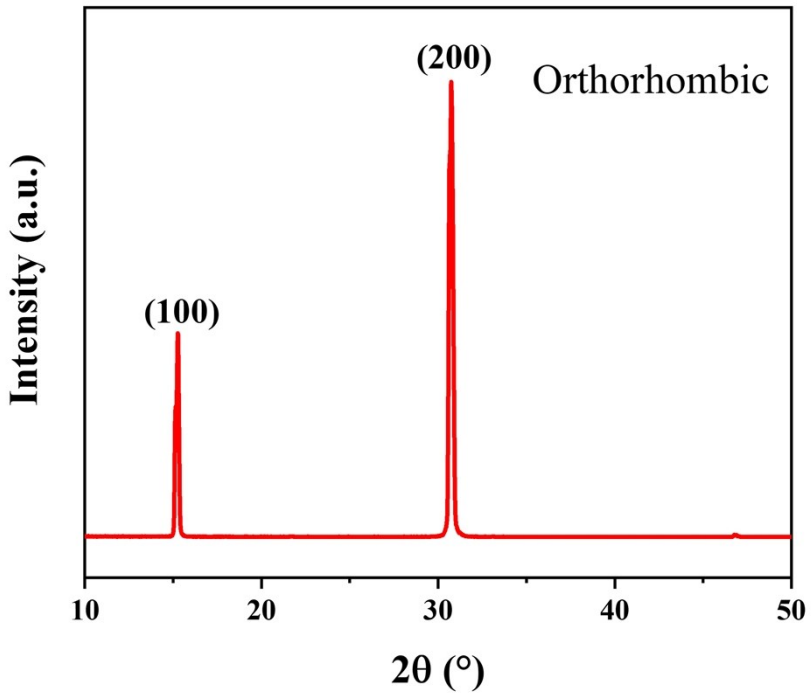

Figure S3. X-ray diffraction pattern of the as-grown $CsPbBr_3$ MPs.

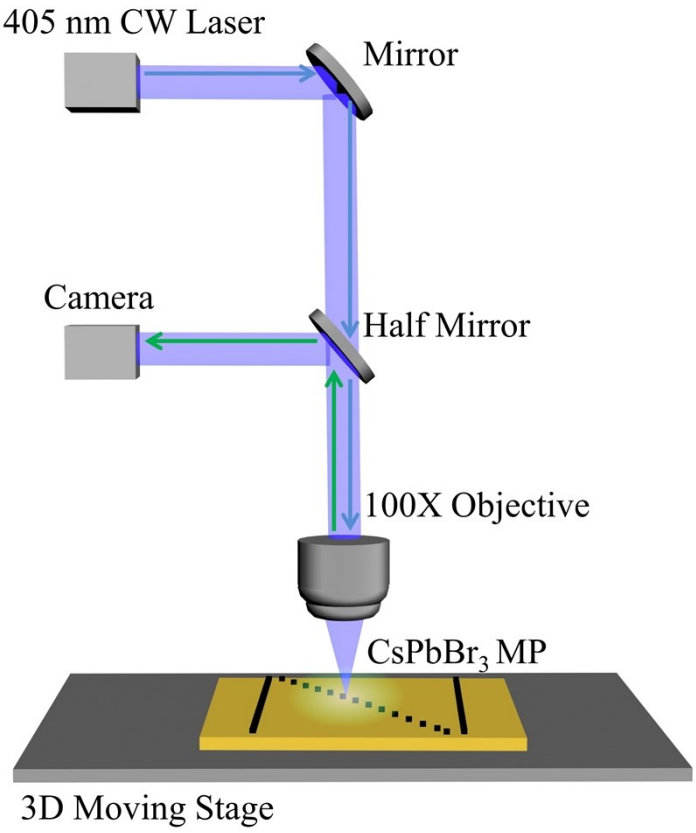

Figure S4. Schematic of the DLW setup.

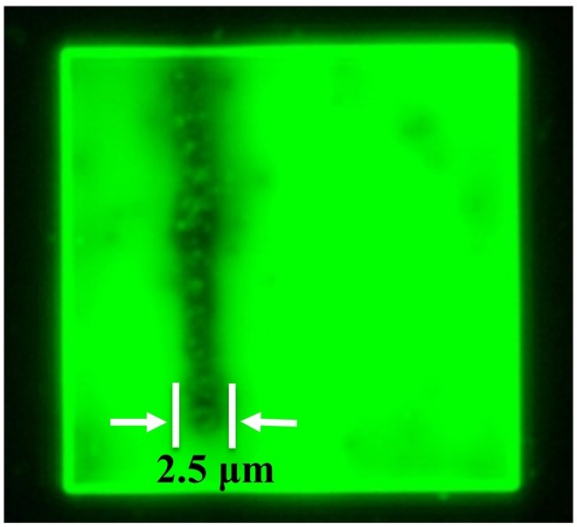

Figure S5. FM image of a "line" patterned $CsPbBr_3$ MP, showing the spatial resolution of a single linewidth is about 2.5 µm.

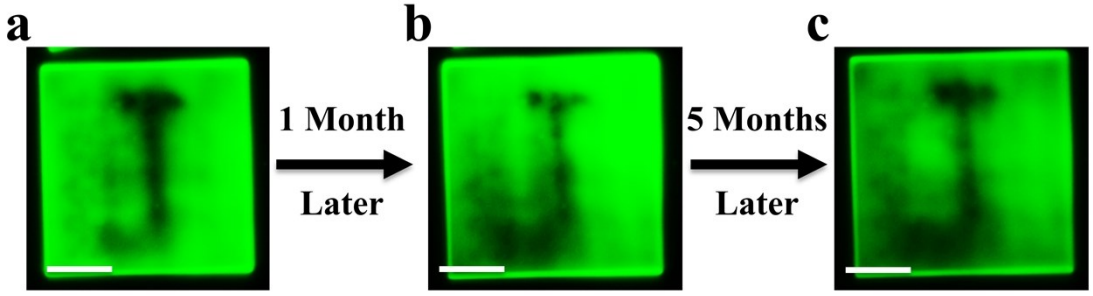

Figure S6. FM images of the "J" patterned $CsPbBr_3$ MP during storage, newly written (a), after storage for 1 month (b), and after storage for 5 months (c). All the scale bars are 10 μm.

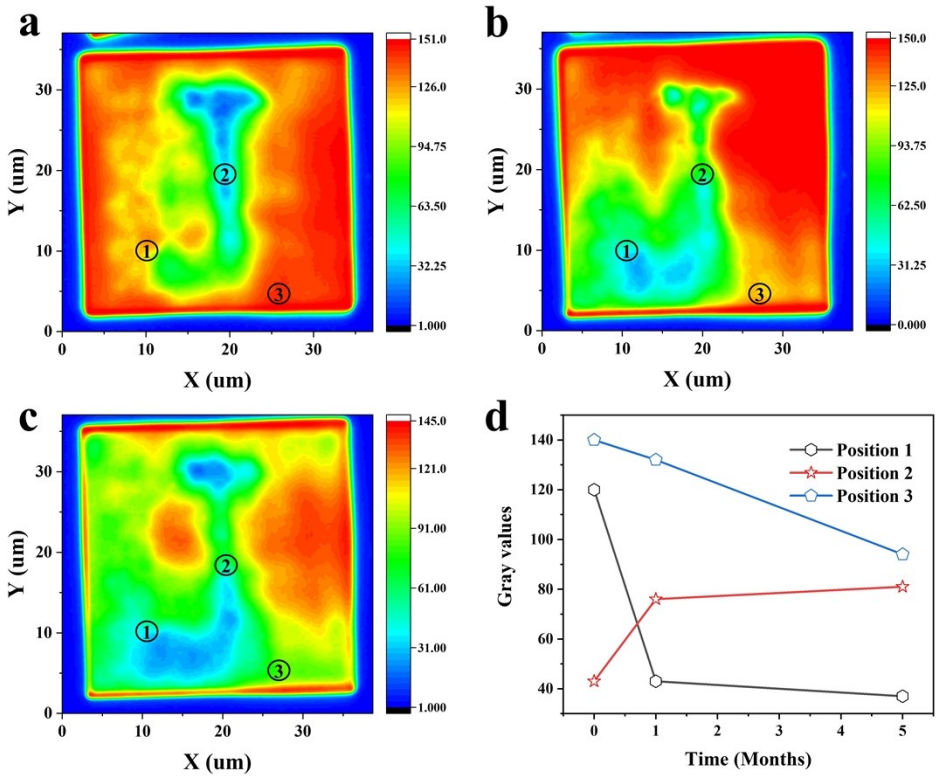

Figure S7. (a-c) Grayscale mappings of the "J" patterned $CsPbBr_3$ MP during storage, newly written (a), after storage for 1 month (b), and after storage for 5 months (c). (d) The gray values of three typical positions.

As shown in the elemental mappings (**Figure S8**), there are no apparent changes after DLW, which indicates the "dents" are too shallow to change the elemental distribution, compared to the thickness of $CsPbBr_3$ MPs (1 μm). For XRD measurement, the crystal powders were collected from the substrates and thoroughly treated with similar DLW laser conditions. As shown in **Figure S9**, the corresponding XRD pattern is noisy due to the deterioration of crystallinity. No new phase appears. Moreover, we prolonged the DLW time until an apparent "dent" appeared on $CsPbBr_3$ MP surface. The confocal micro-Raman experiments were carried out. As shown in **Figure S10**, the Raman spectra of pristine region and laser treated region show no obvious difference, implying no new phases appear.

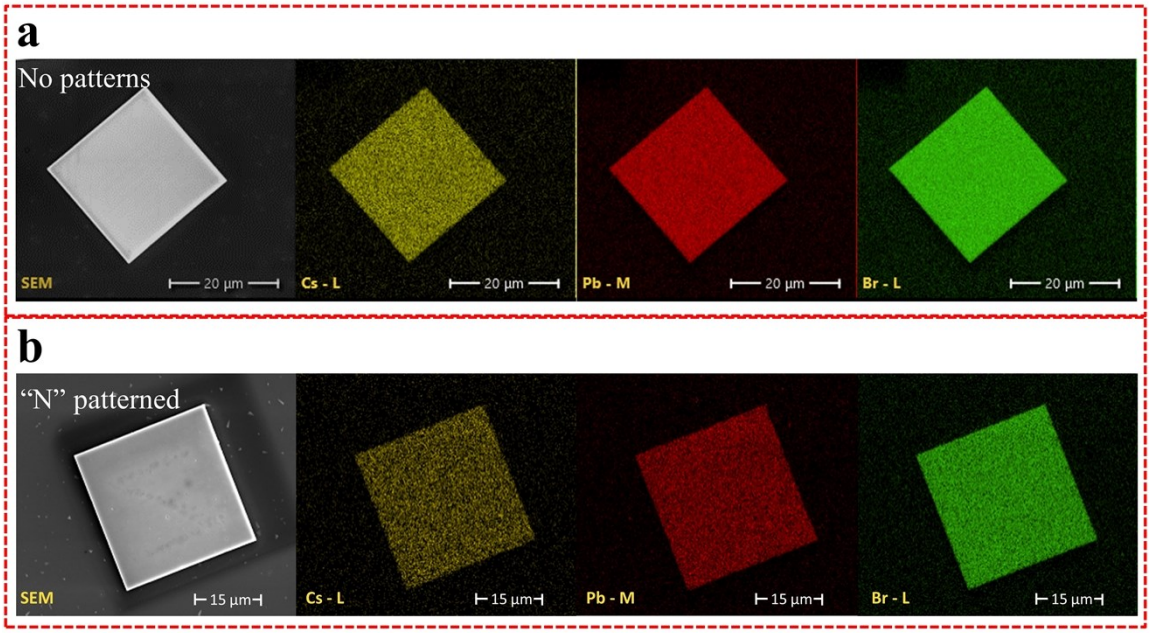

Figure S8. Composition analysis of a single $CsPbBr_3$ MP. EDS mappings of a single MP before (a) and after DLW (b).

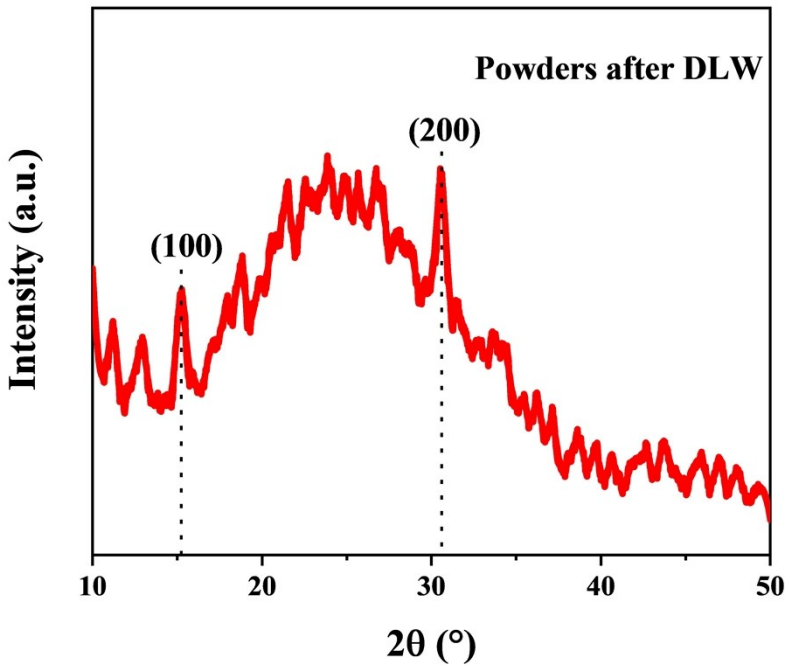

Figure S9. XRD pattern of the $CsPbBr_3$ MPs powders after DLW treatment.

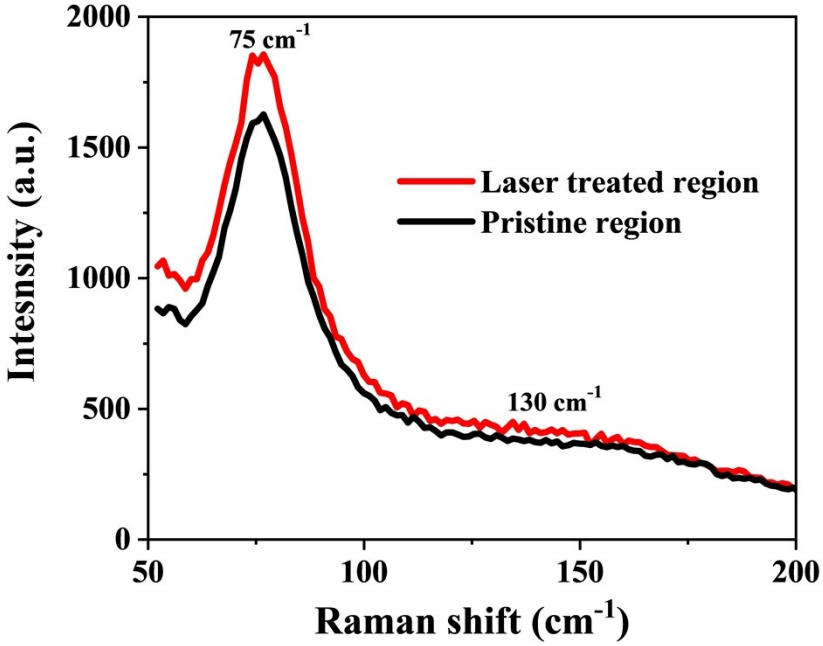

Figure S10. Raman spectra of the pristine and DLW modified regions on the $CsPbBr_3$ MP.

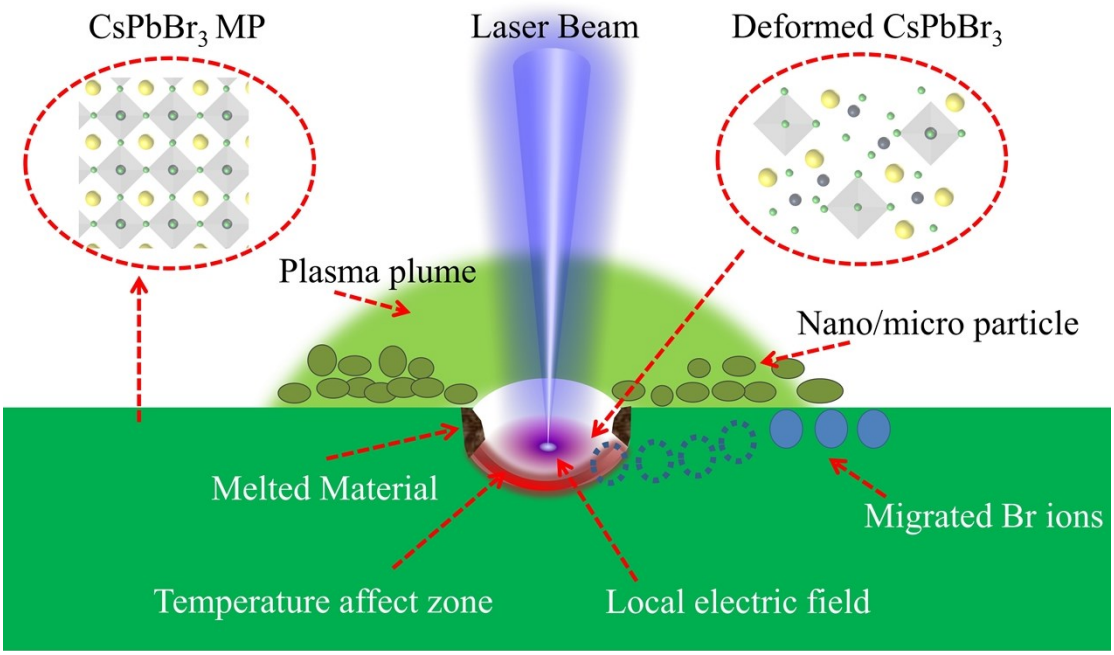

Figure S11. Schematic of the light-matter interactions during the DLW processing on the $CsPbBr_3$ MPs.

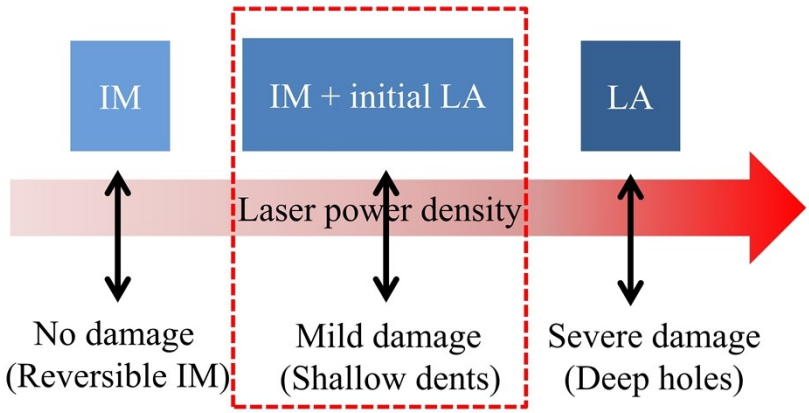

Figure S12. Schematic of different laser ablation degrees, IM= ion migration; LA= laser ablation.

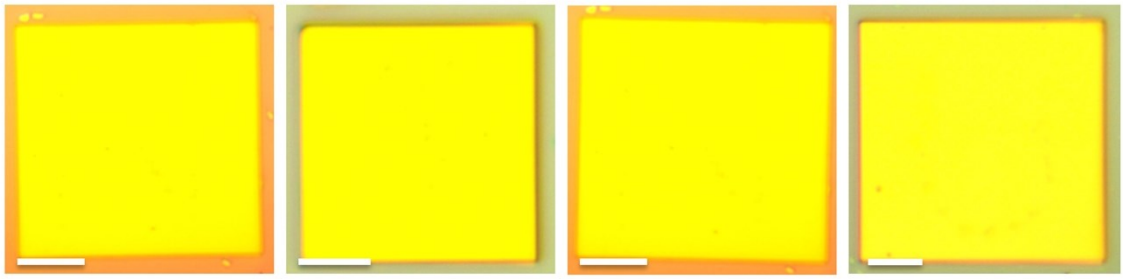

Figure S13. OM images of the "N", "J", "N", and "U" pattered $CsPbBr_3$ MPs. The patterns cannot be observed in the OM images. All the scale bars are 10 μm.

As shown in Figure S14a, the DLW method is applied to $CsPb(Br/I)_3$ MPs. Under the continuous laser irradiation, the original 570-nm emission gradually vanishes and a 690-nm emission gradually appears in 300 seconds, corresponding to mixed Br/I phase and I-rich phase, which is known as the irradiation induced phase segregation.[1,2] The PL intensities of two phases versus irradiation time are shown in Figure S14b. After DLW process, the OM images of the $CsPb(Br/I)_3$ MP show no differences (Figure S14c, d). However, as shown in Figure S14e, f, a large area of red fluorescence appears instead of PL quenching, causing the inhomogeneous luminescence on the surface of the $CsPb(Br/I)_3$ MP, which hinders the application in patterning and micro-encryption.

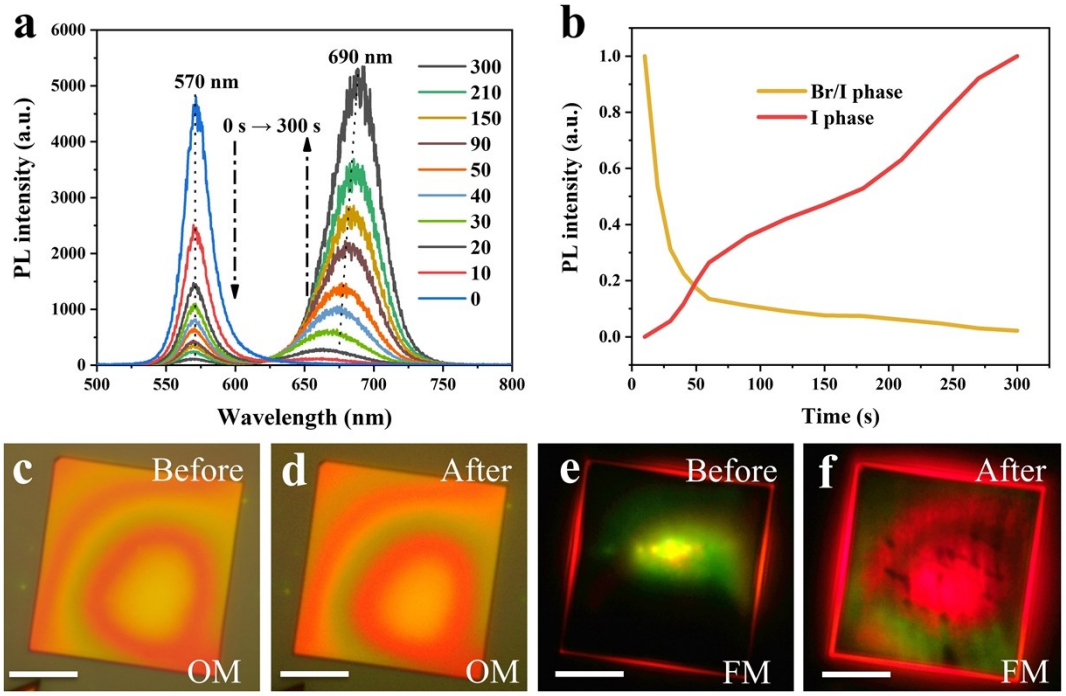

Figure S14. (a) Steady-state PL spectra of the $CsPb(Br/I)_3$ MP during continuous laser irradiation (178 mW). (b) PL intensities of the Br/I phase and I-rich phase versus irradiation time. (c, d) OM images of the $CsPb(Br/I)_3$ MP before and after DLW. (e, f) FM images of the $CsPb(Br/I)_3$ MP before and after DLW. All the scale bars are 10 μm.

As shown in Figure S15a, under the continuous laser irradiation, the fluorescence of RPPs quenches quickly. In 30 seconds, the PL intensity reduces to 15% (Figure S15b). After DLW treatment, RPPs substantially degrade, and the ruined area is much larger than the laser spot, which is clearly seen in both OM and FM images (Figure S15c, d, e, f). The RPPs are unstable under high-power density laser excitation due to their organic-inorganic hybrid structures. Therefore, this DLW method is not feasible for $(C_4H_9NH_2)_2PbI_4$ RPPs.

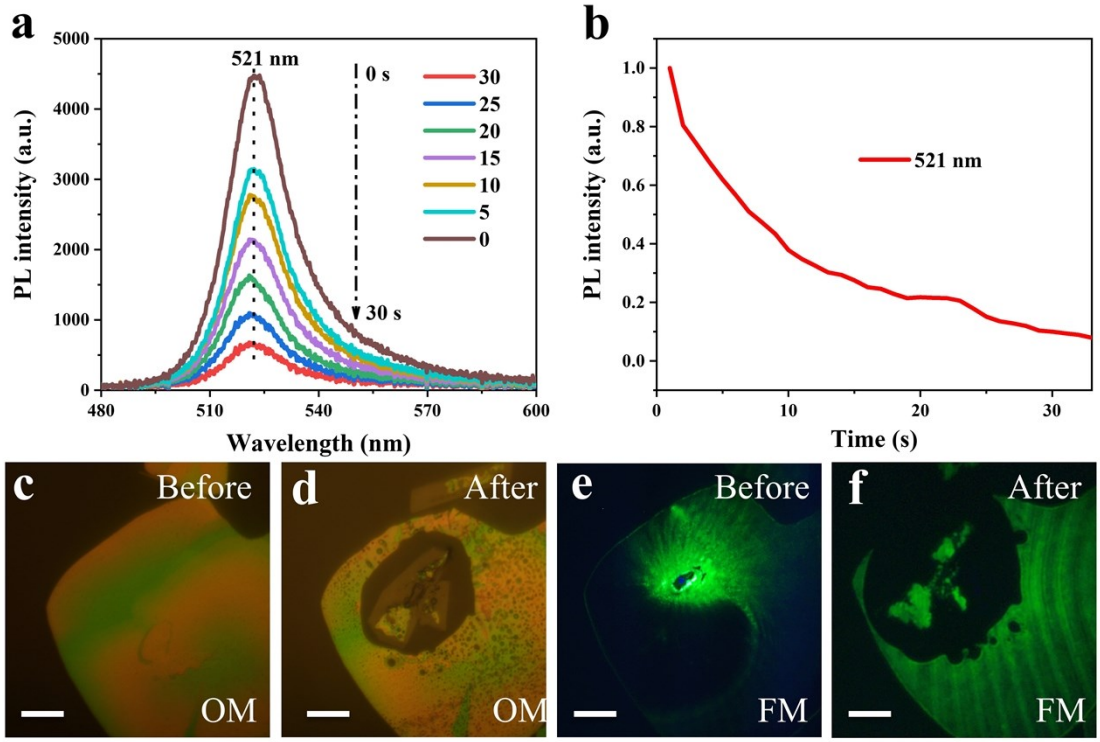

Figure S15. (a) Steady-state PL spectra of the $(C_4H_9NH_2)_2PbI_4$ Ruddlesden-Popper perovskites (RPPs) during continuous laser irradiation of 178 mW. (b) PL intensity of 521-nm emission versus irradiation time. (c, d) OM images of $(C_4H_9NH_2)_2PbI_4$ RPPs before and after DLW. (e, f) FM images of $(C_4H_9NH_2)_2PbI_4$ RPPs before and after DLW. All the scale bars are 10 μm.

Supplementary Note 1. A quantitative estimation of defect density

A quantitative estimation of defect density is conducted based on the model by Snaith et al.[3] The transient population of electrons can be described by,

$$\frac{\partial n(z,t)}{\partial t} = G - D_n\frac{\partial^2 n(z,t)}{\partial z^2} - R_r - R_{nr}, \qquad (1)$$

where G is the carrier generation rate, D_n is the diffusion constant, z is

spatial position, R_r and R_{nr} are the radiative and non-radiative recombination rate. The radiative recombination rate R_r can be described by,

$$R_r = B\left(n(z,t)p(z,t) - n_i^2\right), \quad (2)$$

where B is the radiative recombination constant, $n(z,t)$ and $p(z,t)$ are the electron and hole densities, respectively, while n_i is the intrinsic carrier density. Due to the large bandgap of $CsPbBr_3$ MPs, n_i is negligible at room temperature, and therefore,

$$np - n_i^2 \approx np, \quad (3)$$

Thus, Equation (2) can be simplified as:

$$R_r \approx B(\Delta n + n_0)(\Delta p + p_0), \quad (4)$$

where Δn and Δp are the excess charge carrier densities generated by photoexcitation, while n_0 and p_0 are steady-state carrier densities. Since $\Delta n = \Delta p$, Equation (4) can be further simplified and the complete recombination rate for electrons can be described by the following expression:

$$R_r \approx B\left(\Delta n^2 + \Delta n p_0\right). \quad (5)$$

We assume that the quasi-steady state concentration of trapped electrons gives rise to an excess hole density (p_0), which is regarded as the defect density.

As shown in Figure 2d, the PL lifetimes range from 20 ns to 45 ns, we estimate defect densities range from 4.91×10^{15} cm^{-3} to 8.26×10^{16} cm^{-3}

(using a radiative recombination constant value of $B = 5\times10^{-10}$ cm^{-3} s^{-1} [ref.4]). Our estimated values are relatively rough due to the simplified models and uncertainty of B coefficient.

As shown in Figure 5a, after DLW process, PL lifetime decreased to 1.82 ns, by Equation (5), thus the defect density is about 6.01×10^{17} cm^{-3}. Note the PL lifetimes shown in Figure 2 and Figure 5 are measured at different excitation densities.

References

1 H. Zhang, X. Fu, Y. Tang, H. Wang, C. Zhang, W. W. Yu, X. Wang, Y. Zhang and M. Xiao, *Nat. Commun.* 2019, **10**, 1088.

2 J. R. Vicente and J. Chen, *J. Phys. Chem. Lett*. 2020, **11**, 1802-1807.

3 B. Wenger, P. K. Nayak, X. Wen, S. V. Kesava, N. K. Noel and H. J. Snaith, *Nat. Commun*. 2017, **8**, 590.

4 Y. Yang, M. Yang, Z. Li, R. Crisp, K. Zhu and M. C. Beard, *J. Phys. Chem. Lett*. 2015, **6**, 4688-4692.